Eur. Phys. J. Special Topics **223**, 497–509 (2014)

DOI: 10.1140/epjst/e2014-02105-3

THE EUROPEAN PHYSICAL JOURNAL SPECIAL TOPICS

Regular Article

A phase field crystal study of heterogeneous nucleation – application of the string method

R. Backofen[a] and A. Voigt

Institut für Wissenschaftliches Rechnen, TU Dresden, Germany

Received 13 December 2013 / Received in final form 10 January 2014
Published online 28 February 2014

Abstract. We use the simplified string method in order to examine two dimensional heterogeneous nucleation at a wall and on a substrate. The material is described by a phase field crystal model and the influence of the wall or substrate is included by an external potential. Tuning the external potential we show that we can control the contact angle in equilibrium and misfit to a substrate. The nucleation barrier is reduced by a wall, but cannot be explained by classical nucleation theory due to non-classical nucleation paths. For small misfits a substrate also decreases the nucleation barrier, while large misfits increases the nucleation barrier.

1 Introduction

In heterogeneous nucleation the nucleation process in the liquid is influenced by a wall or a substrate the liquid is in contact with. It is a classical problem in materials science, but it is also of growing interest, due to emerging technological applications in nanopatterning. The nucleation barrier is typically reduced if compared with homogeneous nucleation, which allows to control the nucleation process by tuning the wall or the substrate properties. The barrier reduction is due to an initiated ordering in the liquid phase, which enhances the formation of a crystal. Various theoretical and numerical approaches have been used to understand these physical phenomena.

In classical nucleation theory for an undercooled liquid, the interaction of a crystal in a liquid phase at a wall is completely governed by the surface energies due to liquid-wall γ_{lw}, solid-wall γ_{sw} and liquid-solid γ_{ls} contact, see Fig. 1. The crystal-liquid interface forms a contact angle at the triple junction. For isotropic surface energies the contact angle Θ obeys Youngs law: $0 = \gamma_{\mathrm{lw}} - \gamma_{\mathrm{sw}} - \gamma_{\mathrm{ls}} \cos(\Theta)$. That is, if liquid is favored at the wall the contact angle is above 90°, while preference of solid leads to a contact angle less then 90°. In general, the contact to the wall reduces the nucleation barrier W by a catalytic potency factor $W_{\mathrm{hetero}} = f(\Theta) W_{\mathrm{homo}}$. In the isotropic case, the solid forms a spherical cap and the catalytic factor is defined in two dimensions by $f(\Theta) = \frac{1}{\pi}(\Theta - \frac{1}{2} sin(2\Theta))$, see [1,2]. In three dimensions and for anisotropic surface energies details change but similar results are obtained [2]. While this approach

[a] e-mail: rainer.backofen@tu-dresden.de

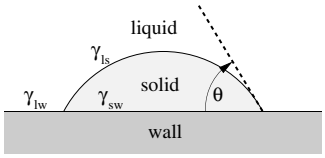

Fig. 1. Sketch of a solid at wall in equilibrium. The shape is governed by the (isotropic) surface energies γ. The contact angle Θ obeys Youngs law.

may quantitatively describe heterogeneous nucleation on a macroscopic length scale, it loses its applicability for smaller nuclei. Here phase field models have been successfully applied, see e.g. [3–6]. These approaches can quantitatively predict nucleation barriers for systems where the necessary input data are available. Unfortunately this is not the case in most situations.

The second setting, nucleation on a substrate, is related to the nucleation of islands in epitaxy. A typical modeling approaches is mean field rate equation theory in which the nucleation rate is described as a function of the mean residence time of an adatom on an island and the probability that two adatoms meet before one of them leaves the island, see [7,8] for the model and [9] for a realization for island growth. The resulting nuclei are always circular and placed at the position of maximal adatom density, which corresponds to the center of the existing island. Also for this problem phase field models have been used, see e.g. [10,11]. A detailed modeling of the nucleation process taking into account the interaction with the crystalline structure of the substrate has not been considered, and will also be subject of this article. We will here concentrate on liquid phase epitaxy (LPE).

We here consider an approach, the phase field crystal (PFC) model, which can be applied for both settings and does neither requires the surface energies as input, nor needs to specify boundary conditions for the phase field variable at the wall or substrate.

The PFC model was introduced as a phenomenological model for solid state phenomena on an atomic scale [12,13]. However, it can also be motivated and derived through classical density functional theory, [14,15]. It has been used in various applications, see e.g. the reviews [16,17] and the references therein. The description of real material requires various extensions, see e.g. [18,19]. In the present study we are not interested in a specific material, but a general concept and therefor restrict ourselves to the non-dimensionalized prototype PFC model, as defined in [14]. It is based on the Swift-Hohenberg free energy

$$\mathcal{F}[\varphi] = \int \frac{\varphi}{2}\left(r + (1+\Delta)^2\right)\varphi + \frac{\varphi^4}{4} + V_{\text{ext}}\,\varphi \,\mathrm{d}x. \tag{1}$$

φ can be interpreted as a rescaled density deviation from a reference, r is a parameter related to temperature and V_{ext} describes an external potential. The evolution equation follows as the H^{-1} gradient flow

$$\frac{\partial \varphi}{\partial t} = \Delta\mu \tag{2}$$

$$\mu = \frac{\delta \mathcal{F}[\varphi]}{\delta \varphi} = r + (1+\Delta)^2\varphi + \varphi^3 + V_{\text{ext}}$$

with the chemical potential μ. This equation minimizes the free energy in phase space. Hence, a stationary solution of Eq. (3) corresponds to a stable or metastable state, e.g. liquid or crystalline state. There are some methods in order to describe the influence of a wall. Structured walls can be modeled by an external potential forcing part

of the solution of φ mimicking the wall [4,20,21] and it was shown that Dirichlet boundary conditions, chosen separately for liquid and crystalline state, can control the contact angle at a wall for an extended PFC [22]. In this work, the external potential is used in order to model the interaction with an unstructured wall or a substrate. We are here interested in nucleation and want to compute nucleation barriers. We are therefor interested in the smallest energy needed in order to go from the liquid to the crystalline state. This path of minimum energy (MEP) connects liquid and crystalline state and is invariant under the prescribed dynamics of Eq. (3). Keeping this in mind, we interpret the right hand side of Eq. (3) as a generalized thermodynamic force. So called chain of state methods [23], such as the nudged elastic band method [24] or the string method [25,26] exploit this property in order to find the MEP, respectively the saddle point. We will here use this approach to determine nucleation barriers in the same way as already considered for homogeneous nucleation [27]. Thereby a path connecting two (meta)stable states is represented by a discrete set of states in phase space and is evolved according to Eq. (3) until the path becomes invariant. The available methods are distinguished by technical details to prevent clustering of the states. We will use the simplified string method (SSM) [28]. In the string method (SM), the dynamics applied to the states representing the path is projected to the normal of the path. Thus, tangential component of the thermodynamic force are neglected. Furthermore, the quality of the representation of the path is assured by moving the states tangentially along the path. SSM avoids a direct projection of the thermodynamic force and leads to a simple algorithm solving Eq. (3) for every state and interpolating between the states along the path. In [28] it is shown that SSM not only simplifies SM but also leads to a more stable and accurate method. Details of the application of SSM to PFC and an extension towards a fixed length SSM (FLSSM) can be find in [27] and will be briefly reviewed below.

In the following we describe the external potential to model wall and substrate interactions, introduce an image processing algorithm to extract the shape of crystallites and the contact angle, describe the details of FLSSM and the implementation of the PFC model and discuss the results.

2 Model and method

2.1 External potential in PFC

Equation (1) considers two different external potentials $V_{\text{ext}} = V_{\text{wall}}$ and $V_{\text{ext}} = V_{\text{sub}}$, one to describe the interaction with a wall and one for the interaction with a substrate. The interaction with a wall is described by

$$V_{\text{wall}} = V_0 \left[\frac{x - w}{w} \right]^{20}, \tag{3}$$

motivated by [29]. V_0 is the interaction strength and w corresponds to the interaction width of the potential. Perpendicular to the wall a density wave is induced by the potential. The increasing potential towards the wall lead to a decreasing φ. Dependent on the strength of the potential φ may decrease without a bound at the wall. This shows two possible problems. The free energy derived by classical density functional theory, which is the basis for the derivation of PFC, assumes that φ is a small scaled density fluctuation from a reference density [14]. Thus, φ should be naturally bound from below. This can be accounted for by adding

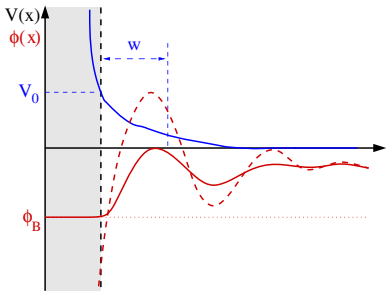

Fig. 2. Sketch of the wall interaction potential, which induces a decaying density wave at the wall.

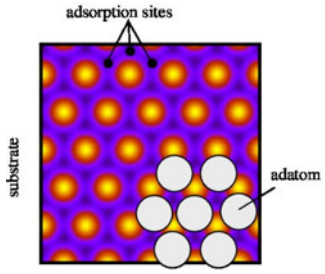

Fig. 3. The pinning potential due to a rigid hexagonal packed substrate leads to 3-fold adsorption sites. The adatom correspond to a particle in solid state modeled by PFC.

a constraint of positive density to the free energy, as e.g. considered in [30]. Additionally, φ at the wall is no longer a small deviation and the assumptions made become questionable. Nevertheless, by choosing V_0 moderate we can define an effective wall interaction, which allows us to control the contact angle of a crystalline phase at the wall in a liquid surrounding. Figure 2 illustrates these problems and their solution.

The interaction with a rigid substrate can be modeled by a pining potential. Here, V_{sub} is motivated by the approximative one mode solution of PFC, see [13], which describes a hexagonal packed surface with lattice distance a,

$$V_{\text{sub}} = V_0 \left(\cos(kx) \cos\left(\frac{ky}{\sqrt{3}}\right) - \frac{1}{2} \cos\left(\frac{2ky}{\sqrt{3}}\right) \right) \tag{4}$$

where $k = \frac{2\pi}{a}$. Again, V_0 is the interaction strength. $V_0 < 0$ leads to binding in the threefold adsorption sites, see Fig. 3. By varying the lattice distance of the substrate elastic stresses are modeled. In the PFC model the potential induced a preordering of the liquid. The density of the liquid, that is the probability of finding a particle, is increased at the adsorption sites and decreased elsewhere.

2.2 Numerical scheme for PFC

The sixth order PFC model in Eq. (3) is solved as a system of second order equations simultaneously and the nonlinear parts are linearized in time. The approach is described in detail in [31]. The finite element discretization uses 4th order Lagrangian elements and is implemented in the finite element toolbox AMDiS [32].

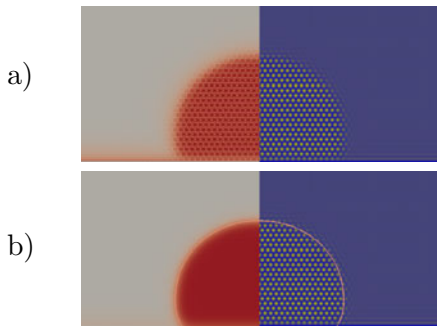

Fig. 4. Identification of the envelope. Right hand side shows a typical density field for a crystal at a wall on the bottom. a) shows the result of applying the indicator, Eq. (5). b) shows the segmentation result Ψ on the left hand side. The shown isoline is the envelope.

2.3 Envelope

In order to interprete contact angles or shapes of crystals from our PFC simulations we need to find the envelope of a crystal. The density fluctuates at the scale of particle distance, but the envelope has a smooth representation of the interface between solid and liquid. We apply a segmentation algorithm from image processing in order to identify the crystal. First a indicator is defined which has to separate the liquid from the crystal state:

$$I = \begin{cases} 1 & \varphi > \varphi_{\text{high}} \text{ or } \varphi < \varphi_{\text{low}} \text{ or } |\nabla\varphi| > c_{\text{high}} \\ 0 & |\nabla\varphi| < c_{\text{low}} \text{ and } \varphi \approx \varphi_{\text{liquid}} \\ & \text{else linear interpolation} \end{cases}, \tag{5}$$

where $\varphi_{\text{high/low}}$ and $c_{\text{high/low}}$ are thresholds for high and low density resp. density gradients. The indicator function identifies the crystal by locally high or low density and high density gradients. The liquid phase is identified assuming the density to be near the liquid density and a small density gradient. In between these thresholds a linear interpolation is applied.

Figure 4(a) shows that this indicator already gives a good but noisy representation of the crystal. In a second step, minimization of a Mumford-Shah energy is used to smooth the representation [33]. The Mumford-Shah energy reads,

$$E[\Psi] = \int \left\{ (I - \Psi)^2 + |\nabla\psi|^2 + \psi^2 (1 - \Psi) \right\} \mathrm{d}x,$$

and is minimized by a field that smoothes the indicator field, see Figure 4(b). The envelope is then defined as the 0.5 isoline of Ψ. The method is quite robust for large crystals and described in more detail in [34].

2.4 Fixed length simplified string method

A path in phase space γ is discretized by an ordered set of states, φ_i:

$$\gamma = \{\varphi_i : i = 0, 1, \ldots, N\} =: \{\varphi_i\}.$$

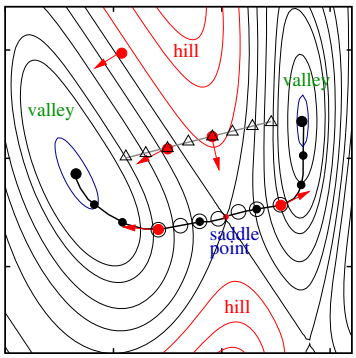

Fig. 5. Sketch of phase space and energy landscape with two (meta)stable states in the valleys. Δ: states of the initial string. (red arrow): generalized thermodynamic forces on the states. (Closed circles) states of the MEP, thermodynamic force is tangential to MEP. (Open circles) states of a string with restricted length and part of the MEP.

This is called the string. The length of the string is defined by

$$L(\gamma) = \sum_{i=0}^{N-1} |\varphi_{i+1} - \varphi_i| \quad \text{and} \quad |\varphi| = \int |\varphi(r)|\, dr$$

where $|\cdot|$ measures the distance between two states and is defined by the L^2-norm. The SSM consists of two steps, an evolution and a reparameterization step, which have to be iterated until the conditions for the MEP is achieved, [25,27,28].

Evolution step: Every state of the string is evolved according the generalize thermodynamic force, Eq. (3).

$$\gamma^n \to \tilde{\gamma}^{n+1} = \left\{\tilde{\varphi}_i^{n+1}\right\} \tag{6a}$$

$$\text{with} \qquad \tilde{\varphi}_i^{n+1} = \tau \Delta\mu + \varphi_i^n. \tag{6b}$$

The evolution of the states in Eq. (6b) is just the finite difference discretization in time of the standard dynamics, Eq. (3) with τ a virtual time step. All states would converge to one of the (meta) stable states, e.g. one of the endpoints of the string. Therefor, a correction step is needed.

Reparameterization step: In order to maintain a good representation of the path the states are redistributed.

$$\tilde{\gamma}^{n+1} \to \gamma^{n+1} = \left\{\varphi_i^{n+1}\right\} \tag{7}$$

$$\text{such that } \left|\varphi_{i+1}^{n+1} - \varphi_i^{n+1}\right| = \frac{L(\tilde{\gamma}^{n+1})}{N-1} \quad i = 0, 1, \ldots, N-1$$

and γ^{n+1} and $\tilde{\gamma}^{n+1}$ representing the same path in phase space. The redistribution is done by linear interpolation between the states of the evolved path $\tilde{\gamma}^{n+1}$.

The aim of FLSSM is to concentrate the states near the saddle point [27]. That is, the length of the string on both sides of the saddle point is restricted to a fixed length. This is achieved by a modification of the reparametrization step [27]. First quadratic interpolation is used to shift the state of maximum energy to the saddle

point. Then the standard reparametrization step relative to the approximative saddle point is used.

$$\tilde{\gamma}^{n+1} \to \gamma^{n+1} = \left\{\varphi_i^{n+1}\right\} \tag{8}$$

$$\text{such that } \left|\varphi_{i+1}^{n+1} - \varphi_i^{n+1}\right| = \frac{L_\mathrm{l}}{N_\mathrm{l} - 1} \quad i = 0, \ldots, N_\mathrm{l}$$

$$\text{and } \left|\varphi_{i+1}^{n+1} - \varphi_i^{n+1}\right| = \frac{L_\mathrm{r}}{N_\mathrm{r} - 1} \quad i = N_\mathrm{r} + 1, \ldots, N,$$

where $L_{\mathrm{l,r}}$ and $N_{\mathrm{l,r}}$ are the prescribed string length resp. the number of states left and right from the energy maximum. Consequently, the ends of the string are not reaching the stable states. The stable states are easily achieved afterward by minimizing the energy using the ends of the strings as an initial condition. In our case the liquid state is quite near the saddle point.

3 Result

We examine heterogenous nucleation in two dimensions for two possible set-ups: Nucleation in a two dimensional liquid bounded by a wall, see Sect. 3.1. Here we can compare our results with the classical theory for the contact angle. The second approach considers nucleation of islands in a two-dimensional liquid on a rigid structured substrate, see Sect. 3.2. Here we will analysis the influence of elastic misfits on the nucleation barrier.

3.1 Nucleation on a wall

We consider first the equilibrium crystal shape at a wall and analysis the influence of the contact angle on the wall interaction potential.

We choose the PFC model to be in the solid-liquid coexistence region, $(r,\, \bar{\varphi}) = (-0.25, -0.32)$ [13]. For these parameters the anisotropy of the solid-liquid surface tension is very small and circular equilibrium shapes are obtained [35]. On the bottom side of the simulation domain the wall interaction V_wall in Eq. (3) is introduced. In a pure liquid phase this leads to a density wave perpendicular to the wall. Adding some localized distortion to the liquid state, the liquid and crystalline phase separate and a crystal is formed at the wall, which relaxes towards its equilibrium, see Fig. 4 for a typical example. We determine the contact angle as a function of the interaction strength V_0 and the interaction width ω, see Fig. 6 for the computed equilibrium shapes and Fig. 7 for the corresponding contact angles. The contact angle is measured as the slope of a tangent fitted to the envelope near the wall. The first layer is distorted by the interaction potential and in the same way the envelope is hard to define. Thus, the tangent is fitted at the second layer which leads for large grains to a negligible systematic error. Numerical experiments varying the fitting procedure and treating the envelope at the wall show that the contact angle can be determined approximately by $\pm 4\%$ for grains as large as shown in Fig. 4. The shape of small grains are dominated by the first atomic layer and the atomic structure of the grain, e.g. Fig. 9. Thus, a reasonable macroscopic contact angle could not be obtained for small grains.

For a fixed interaction width ($\omega = 5$) we obtain wetting angles below 90°. A 90° contact angle would be expected as the limit of a vanishing interaction strength which corresponds to a set-up without a wall. Increasing V_0 leads to a decreasing contact angle until a minimum of 75° at $V_0 = 0.4$ is reached. Further increasing V_0

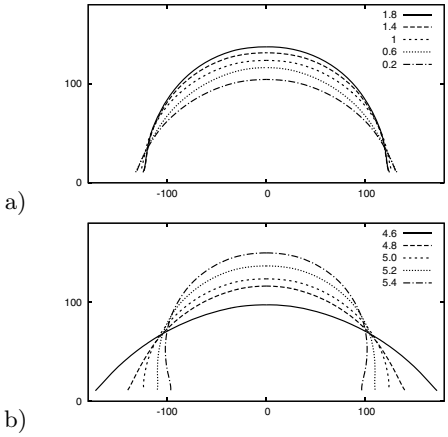

Fig. 6. Computed equilibrium shapes for a) various interaction strength V_0 and constant width $\omega = 5$ and b) various interaction width ω and constant strength $V_0 = 1$.

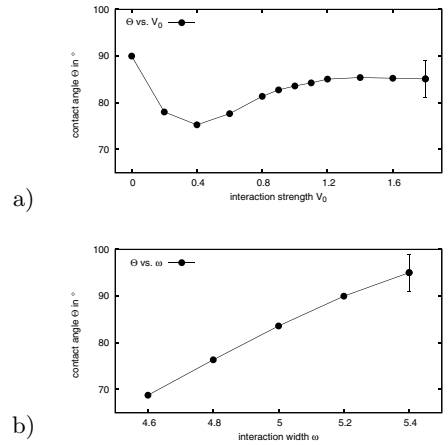

Fig. 7. Corresponding contact angle of the equilibrium shapes in Fig. 6. a) Variation of interaction strength V_0 ($\omega = 5$). b) Variation of interaction width ω (V_0=1). The error is approximated by numeric tests using slightly different methods defining the envelope at the first solid layer.

increases the contact angle again towards a plateau at around 85°. Contact angles above 90° can not be achieved by varying V_0. The contact angle is more sensitive to the interaction width. Keeping the interaction strength fixed ($V_0 = 1$) and varying the interaction width, contact angles above 90° can also be achieved. A variation of interaction width from 4.6 to 5.4 leads to contact angles between 68° and 95°. The contact angle increases with increasing interaction width until the crystal finally detaches from the wall.

The used wall interaction introduces always a repulsive force to the particles, leading to a decrease of the mean density towards the wall. According to the phase diagram a decreasing mean density leads to an increase of the free energy difference between liquid and crystalline state. Thus, a locally reduced density prefers the liquid state and a contact angle above 90° is expected. However, for a small interaction width ω the wall potential also induces a decaying density wave perpendicular to the wall, leading to a preordering in the liquid state. The first peak of this density wave

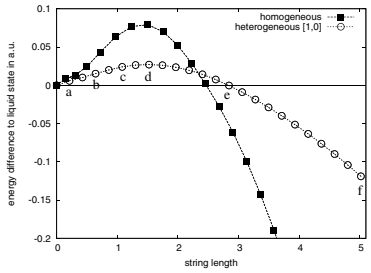

Fig. 8. Energy vs. string length at the MEP. Open symbols describe the MEP for homogeneous nucleation,while closed symbols correspond to the heterogeneous case. The labels a)–f) indicate the states shown in detail, Fig. 9. The wall interaction reduces the nucleation barrier by a catalytic potency factor of 0.34.

increases with decreasing interaction width and already resamples part of the crystalline ordering. The competition of the repulsive force and the induced preordering defines the contact angle and allows angles below and above 90°.

We now examine nucleation at the wall for a contact angle of 94°. From our previous calculation the stable states in phase space are already identified: the liquid in equilibrium and the equilibrium crystal at the wall. The initial string in phase space is constructed by linear interpolation between these stable states and consists of 24 states. First SSM is used to relax the string in phase space. This leads to a rough description of the MEP, which is used as a starting point for FLSSM in order to get a more accurate description. Figure 8 shows the energy vs. string length[1] for the MEP in comparison with homogeneous nucleation.

The wall interaction V_{wall} reduces the nucleation barrier significantly. The states a)–c) correspond to subcritical grains and will decay to the liquid state, d) is the minimum stable grain, while c)–f) are supercritical grains and will evolve towards the equilibrium crystal shape at the wall. The maximum density amplitude in the crystalline increases from state a)–f) but still does not reach the value of the equilibrium shape. Thus, the crystal in all shown states is still not bulk like. The same behavior has been reported for homogeneous nucleation [27] and marks a difference if compared with classical nucleation theory.

The envelope is defined according the maximal amplitude of every state as described in Sect. 2.3. For subcritical grains, a)–c), the difference between the density amplitude in the liquid at the wall and the maximum density is so small that the preordering layer is identified as solid[2]. Thus, for these small grains, the envelope strongly depends on the details of the local structure. A determination of the contact angle is not possible for grains with just a few particles. However, the envelopes emphasizes, that the shape of the grains changes from flat to higher curvature. State d), the minimum stable grain, is relatively flat with broad decay of the density amplitudes, while state e) is more compact with higher density amplitudes. Thus, the shape is changing along the MEP, which indicates that the surface tension of the crystal/liquid interface is not independent on crystal size. A similar dependency has

[1] The string length is the natural coordinate for the string method, but the connection to a macroscopic property (e.g. size of grain) is not trivial. Especially, if the grains are very small as in our case. It should be noted, that string length between different simulations can not be compared.

[2] Another possibility is to use the maximal amplitude of all states, then in case a)–b) no solid at all is identified. We prefer our choice as this gives an idea of the morphology of the region where the phase change starts.

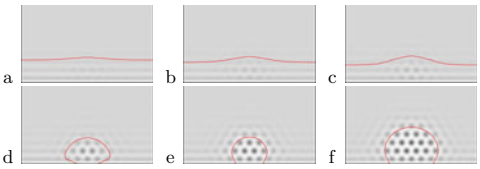

Fig. 9. States along the MEP. a)–f) Corresponds to the states labeled in Fig. 8. The envelope is calculated by image segmentation algorithm as described in Sect. 2.3.

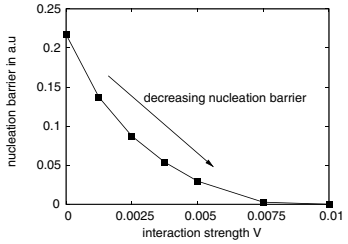

Fig. 10. Nucleation barrier vs. pinning strength on a rigid substrate with the same periodicity.

already been reported in [35]. Again a significant discrepancy if compared with the classical theory.

To summerize the computed nucleation paths near the nucleation barrier are not classical. Thus, we should expect also a discrepancy in the nucleation barrier if compared with the classical theory. For contact angle greater than 90° classical nucleation theory predicts a reduction of the nucleation barrier of 44%. But, here the nucleation barrier is reduced by 76%. Thus the non classical behavior of our nucleation paths lead to further reduction of the nucleation barrier. The contact angle for the minimum stable grain, Fig. 9(d), is hard to define, but the lengthy shape of the nucleus indicate that at this situation a macroscopic contact angle is less than 90°, which would explain the smaller nucleation barrier. But it remains questionable, if the picture of a macroscopic contact angle holds for small grains dominated by the microscopic structure. Contrary, the big grains used to define the contact angle are well defined macroscopically. That is, an envelope can be easily constructed.

3.2 Nucleation on a substrate

The substrate is modeled by the pinning potential V_{sub} in Eq. (4). The liquid state at the substrate is directly influenced by the structure of the pinning potential, a strong pinning at the three fold adsorption sites correspond to high densities in the liquid. We calculate the nucleation barrier as before using FLSSM.

First the underlying substrate has the same periodicity as the two dimensional crystaline solution of PFC. In other words, the crystal modeled by PFC fits to the substrate, there is no misfit. This corresponds to the typical situation considered for epitaxial growth in [7–9] and has already been studied using PFC in [36]. Increasing of the pinning strength leads to an increasing probability of finding particles at the three fold adsorption sites, see Fig. 3.

As before, this can be interpreted as a preordering and leads to a decreasing nucleation barrier. For a strong pinning the nucleation barriers can also vanishes, see Fig. 10.

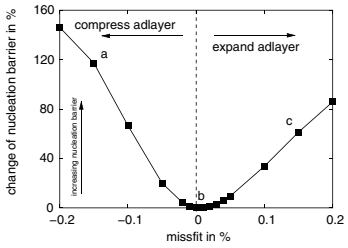

Fig. 11. Nucleation barrier vs. misfit of a rigid substrate.

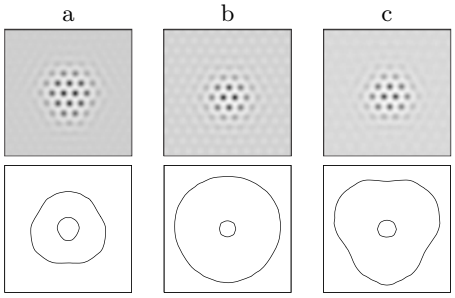

Fig. 12. Shape of minimal stable grain and grain after some growth. Rows a)–c) correspond to misfits labeled in Fig. 11. First column: density distribution of minimal stable grain. Second column: shape of the minimum stable grain and grain after some growth.

We now consider a situation corresponding to heteroepitaxial growth. For a medium pinning strength of $V = 0.0025$ the lattice constant a of the substrate is varied from 20% compression to 20% stretching, see Fig. 11.

Increasing the misfit always increases the nucleation barrier. But the increase is not symmetric. The nucleation barrier is slightly more sensitive to compression. However, a strong influence of the misfit on the nucleation barrier is observed. Only -5% misfit is needed to increase the nucleation barrier by 20%. But also the shape of the nuclei is influenced by the misfit, see Fig. 12. The minimum stable grains contain just a few particles, which has also been found for homogeneous nucleation [27]. Thus, the shape of the grains are hard to define quantitatively. Nevertheless, small misfits below 10% lead to basically round grains. But, higher misfits show quite different shapes, changing from circles to triangles and hexagons. Even if these results are only qualitative they indicate a strong influence of the misfit on island growth, and differ from the classically considered mean field rate equations.

4 Discussion

We studied two set-ups for two dimensional heterogeneous nucleation, nucleation at a wall and nucleation at a rigid substrate. All considered nucleation paths are not classically. That is, the nucleation path can not well described by the macroscopic properties of the material and the process. Instead microscopic effects, such as pre-ordering of the liquid and non bulk-like solids with decreased ordering dominate the nucleation and the structure of the minimum stable grain.

Phase field models shows similar deviations from classical nucleation path if the size of the grain becomes comparable to the interface thickness of the phase field or influence region of the wall [4,5]. Our grains are even smaller. The small size is

due to a weak surface energy resulting from the standard PFC model [18,21,37]. For more realistic situations with higher surface energies, the standard PFC model has to be modified towards higher order terms, as e.g. considered in the eighth order PFC model parameterized for Fe, see [18]. Nevertheless, the represented approach to compute critical nuclei and nucleation barriers using FLSSM can be easily applied to any modification and extension of the PFC model.

Our treatment of the wall and substrate as an external potential is motivated by the derivation of the PFC from classical density functional theory of interacting particles. The corresponding interaction potential can be derived from the microscopic structure and property (interaction strength) of the wall or the substrate. However, in this article the used external potential does not quantitatively connect to the microscopic world, but is chosen to show typical nucleation properties. We controlled the contact angle and showed a non-classical decrease of the nucleation barrier. Interaction with a substrate decreases the nucleation barrier if the structure of the substrate fits the solid, e.g. vanishing misfit, and can even lead to a vanishing nucleation barrier. Increasing the misfit, compression or expansion, leads to higher nucleation barriers. This set up maybe used to control the nucleation process in liquid phase epitaxy and might lead to improved nanopatterning, as e.g. considered in [38].

RB and AV acknowledges support of the DFG via Vo899/7 within SPP 1296.

References

1. K. Fisher, W. Kurz, *Fundamentals of Solidification* (Trans. Tech, Uetikon-Zürich, 1986)
2. C. Herring, *The Physics of Powder Metallurgy* (McGraw-Hill, New York, 1951)
3. L. Gránásy, T. Pusztai, G. Tóth, Z. Jurek, M. Conti, B.R. Kvamme, J. Chem. Phys. **119**, 10376 (2003)
4. L. Gránásy, T. Pusztai, D. Saylor, J. Warren, Phys. Rev. Lett. **98**, 1 (2007)
5. J.A. Warren, T. Pusztai, L. Környei, L. Gránásy, M. Cheng, Phys. Rev. B **79**, 1 (2009)
6. J.F. Lutsko, Phys. Rev. E **74**, 1 (2006)
7. J. Krug, Phys. A **313**, 47 (2002)
8. P. Politi, C. Castellano, Phys. Rev. E **66**, 031605 (2002)
9. R. Backofen, A. Voigt, J. Cryst. Growth **303**, 100 (2007)
10. P. Otto, F. Penzler, A. Rätz, T. Rump, A. Voigt, Nonlinearity **17**, 477 (2004)
11. A. Redinger, O. Ricken, P. Kuhn, A. Rätz, A. Voigt, J. Krug, T. Michely, Phys. Rev. Lett. **100**, 1 (2008)
12. K. Elder, M. Katakowski, M. Haataja, M. Grant, Phys. Rev. Lett. **88**(24), 245701 (2002)
13. K. Elder, M. Grant, Phys. Rev. E **70**, 051605 (2004)
14. K.R. Elder, N. Provatas, J. Berry, P. Stefanovic, M. Grant, Phys. Rev. B **75**, 1 (2007)
15. S.V. Teeffelen, R. Backofen, A. Voigt, H. Löwen, Phys. Rev. E **79**, 1 (2009)
16. H. Emmerich, H. Löwen, R. Wittkowski, T. Gruhn, G.I. Tóth, G. Tegze, L. Gránásy, Adv. Phys. **61**, 665 (2012)
17. H. Emmerich, L. Gránásy, H. Löwen, Eur. Phys. J. Plus **126**(10), 1 (2011)
18. A. Jaatinen, T. Ala-Nissila, Phys. Rev. E **82**, 1 (2010)
19. K.A. Wu, A. Karma, J. Hoyt, M. Asta, Phys. Rev. B **73**, 1 (2006)
20. L. Gránásy, G. Tegze, G.I. Tóth, T. Pusztai, Philosophical Mag. **91**, 123 (2011)
21. G.I. Tóth, G. Tegze, T. Pusztai, G. Tóth, L. Gránásy, J. Phys.: Cond. Matter **22**, 364101 (2010)
22. R. Prieler, J. Hubert, D. Li, B. Verleye, R. Haberkern, H. Emmerich, J. Phys.: Cond. Matter **21**, 464110 (2009)
23. D. Sheppard, R. Terrell, G. Henkelman, J. Chem. Phys. **128**, 134106 (2008)
24. G. Henkelman, H. Jónsson, H. Jo, J. Chem. Phys. **113**, 9978 (2000)
25. E. Vanden-Eijnden, M. Venturoli, J. Chem. Phys. **130**, 194103 (2009)

26. W. Ren, E. Vanden-Eijnden, W.E., Phys. Rev. B **66**, 5 (2002)
27. R. Backofen, A. Voigt, J. Phys.: Cond. Matter **22**, 364104 (2010)
28. W. Ren, E. Vanden-Eijnden, J. Chem. Phys. **126**, 164103 (2007)
29. J. Dzubiella, C. Likos, J. Phys.: Cond. Matter **15**, 147 (2003)
30. S. Praetorius, A. Voigt, Macromol. Theory Simul. **20**, 541 (2011)
31. R. Backofen, A. Rätz, A. Voigt, A. Rätz, Philosophical Mag. Lett. **87**, 813 (2007)
32. S. Vey, A. Voigt, Comput. Vis. Sci. **10**, 57 (2007)
33. D. Mumford, J. Shah, Comm. Pure Appl. Math. **42**, 577 (1989)
34. B. Berkels, A. Rätz, M. Rumpf, A. Voigt, J. Sci. Comput. **35**, 1 (2008)
35. R. Backofen, A. Voigt, J. Phys.: Cond. Matter **21**, 464109 (2009)
36. Y.M. Yu, R. Backofen, A. Voigt, J. Crystal Growth **318**, 18 (2011)
37. A. Jaatinen, C.V. Achim, K.R. Elder, T. Ala-Nissila, Phys. Rev. E **80**, 1 (2009)
38. Y.-M. Yu, A. Voigt, Appl. Phys. Lett. **94**, 043108 (2009)